Electric-field-gradient tensor and boron site-resolved ^{11}B NMR in single-crystalline YB_{12}

Z. Fojud,[1] P. Herzig,[2] O. J. Żogał,[3] A. Pietraszko,[3] A. Dukhnenko,[4] S. Jurga,[1] and N. Shitsevalova[4]
[1]*Institute of Physics, A. Mickiewicz University, Umultowska Street 65, 61-614 Poznań, Poland*
[2]*Institut für Physikalische Chemie, Universität Wien, Währinger Straße 42, 1090 Vienna, Austria*
[3]*Institute for Low Temperature and Structure Research, Polish Academy of Sciences, Okólna Street 2, 50-422 Wrocław, Poland*
[4]*Institute for Problems of Materials Sciences, Academy of Sciences of Ukraine, Krzhyzhanovsky Street 3, 03680 Kiev, Ukraine*
(Received 25 October 2006; revised manuscript received 23 February 2007; published 9 May 2007)

^{11}B NMR measurements on a single crystal of YB_{12} have been performed at room temperature at a frequency of 128.4 MHz. The electric-field-gradient (EFG) tensor components and the principal axes calculated previously by first-principles methods have been verified experimentally. Three magnetically different boron-atom groups in the B_{12} cluster were clearly observed for the crystal orientation used in this work. This distinction results from different EFG-tensor orientations with respect to magnetic field and not from different quadrupolar splittings (ν_Q) or asymmetry-parameter values (η). The magnetically different boron atoms have been identified through the calculated angle dependence of the satellite transitions (0°–360°). Very satisfactory agreement between the calculated and experimental angular dependencies of the EFG tensor has been obtained. Similarly, the quadrupolar splittings and asymmetry parameters agree very well with those previously determined from NMR measurements on a powder sample of YB_{12}.

DOI: 10.1103/PhysRevB.75.184102 PACS number(s): 81.05.Je, 76.60.Gv

I. INTRODUCTION

Nuclear magnetic resonance (NMR) is a microscopic tool well suited to study the electronic structure in metallic borides. From the measured quantities, the spin-lattice relaxation rate and the Knight shift probe the electron density of states (DOS), whereas electric-field gradients (EFGs) are sensitive to electronic charge distributions. Both the DOS and the EFG can be theoretically calculated and compared with the experimental values. In particular, using existing calculation techniques[1–4] for the EFG, very good agreement between theoretical and experimental data is obtained. This explains the large number of studies by ^{11}B NMR in metal borides as well as similar investigations in other systems which already appeared in the literature.[5–10]

In first-order perturbation and for half-integral spin (^{11}B case), the quadrupole interaction of the electric-field gradient with the nuclear-quadrupole moment leaves the central transition ($+1/2 \leftrightarrow -1/2$) unchanged and new components of the spectra termed satellites appear. They are symmetrically displaced about the central transition and their positions depend on the strength of the quadrupole interaction and the orientation of the EFG with respect to the magnetic field. The magnitude of the electric-field gradient at the nucleus is described by a traceless second-rank tensor. With respect to the principal-axes system, the tensor has three components. Their values and the orientation in space of the principal axes can be calculated and experimentally determined by recording absorption spectra. Because of the skin-effect problem, most of the NMR measurements on metal borides were made on powder samples until now.[5–7,9,10] Then only the absolute value of the quadrupole-coupling constant and the asymmetry parameter of the electric-field gradient tensor can be determined. The information on orientation of the principal axes of the tensor with respect to the crystallographic axes is lost.

Both the limited radio-frequency (rf) field penetration (skin effects) due to the metallic character of the metal dodecaborides (to which YB_{12} belongs) and the difficulties in the preparation of single crystals are responsible for the limited number of ^{11}B NMR studies in these materials. Details on the preparation of boride single crystals can be found in the literature (see, e.g., Ref. 11). Earlier single-crystal ^{11}B NMR experiments in metal dodecaborides[12] concern the spin-lattice relaxation rates, $1/T_1$, in YbB_{12}. The measurements of $1/T_1$ were performed for three different crystal orientations versus the magnetic field.

In this paper, we report angle-resolved ^{11}B NMR spectra in a single crystal of YB_{12} together with their interpretation in terms of the EFG tensor at the boron site and its angular dependence. This allows us to compare EFG-tensor components and their orientations, previously calculated[10] by first-principles methods, with corresponding experimental results. It will be shown that although all boron atoms in the unit cell are equivalent, their EFG-tensor angular orientation permits us to distinguish between different boron-atom groups in the B_{12} cluster.

II. EXPERIMENT

The crystal structure of YB_{12} is of NaCl type (space group $Fm\bar{3}m$, No. 225), where the positions of Na and Cl correspond to those of Y and the centers of the B_{12} cuboctahedra, respectively. A single crystal was grown by the floating-zone method. Its real chemical composition has been found to be $Y_{0.90}B_{12}$ using an x-ray microanalyzer. The crystal was cut into a plate ($2.3 \times 4 \times 10$ mm^3) normal to the [410] axis and placed on a goniometer of the NMR probe. The crystal structure, the lattice parameters, and the orientation of the crystal were determined using a single-crystal x-ray four-circle diffractometer. The main directions of the crystal edges were obtained with an accuracy of ±5°. Our standard procedure for orienting the crystal in the external magnetic field of the NMR spectrometer was as follows. A preliminary adjustment of the crystal was performed by determining the right angle between a side plane of the crystal and the transverse plane

of the NMR probe. This was achieved by using a flat rectangular triangle. Then the crystal was centered in the rf coil using a slide caliper. Finally, the angle positions of the crystal were set by a worm gear which rotates the crystal, while the rf coil and the external magnetic field remain fixed. The precision of the angle adjustment, according to the manufacturer of the system (Megatron GmbH), was 1 min per angle degree. At the start of the experiment, the magnetic field $\mathbf{B}_0$ was parallel to the [410] axis before the crystal was rotated in steps of 10° around the [−3 12 1] axis.

The complete ^{11}B NMR spectrum was registered on a Bruker Avance DMX 400 spectrometer using a superconducting magnet of 9.4 T. The collected half of the solid echo signal following a $(\pi/2)_0-\tau-(\pi/2)_{90}$ pulse sequence was subjected to Fourier transformation. The observed Larmor frequency was 128.4 MHz, matching well the $\pi/2$ rf pulse length of 0.9 μs. The distance between the two pulses in the sequence was 28 μs and the repetition time of the sequence was 2 s. In order to increase the signal-to-noise ratio, the echo signals were summed 2048 times. All *RLC* elements in the electronic systems of the probe head together with the solenoid coil and the crystal were kept at constant temperature (25 °C, 298 K). In this way, the thermal surface effects caused by the eddy currents—due to very short rf pulses—have been eliminated.

III. RESULTS AND DISCUSSION

The angular dependence of the spectra is shown in Fig. 1. Each spectrum consists of a central line transition accompanied by pairs of symmetrically distributed satellite transitions. The positions and number of satellite pairs depend on the rotation angle (Fig. 2). The separation between the satellite lines in the pairs is due to first-order quadrupolar interaction. For spin with $I=3/2$, an electric quadrupole moment Q, and for an EFG tensor with a component of maximum absolute value, V_{ZZ}, this separation is

$$\Delta\nu = \nu_Q|(3\cos^2\theta - 1 + \eta\sin^2\theta\cos 2\phi)|, \qquad (1)$$

where $\nu_Q=eQV_{ZZ}/2h$, $\eta=|(V_{XX}-V_{YY})|/|V_{ZZ}|$, and θ, ϕ are the polar angles which are defined by the orientation of the external magnetic field with respect to the principal-axes system of the EFG.

The number of the satellite pairs depends on the number of magnetically nonequivalent boron sites and/or the number of different EFG tensors in the unit cell. According to the crystal structure of YB_{12}, there is only one (48*i*) position for boron[13] and, disregarding orientation, only one EFG tensor.[10] It is, therefore, the orientation of the EFG tensor with respect to the magnetic field that makes the spectrum complex, i.e., there is more than just one satellite pair. We will analyze this aspect closely below.

The crystal structure of YB_{12} is shown in Fig. 3. It illustrates the arrangement of the yttrium atoms and the B_{12} clusters as well as the different inter- and intracuboctahedral B-B bond distances. As mentioned in Ref. 10, the most negative EFG component is related to a principal axis in the direction of the strongest (shortest) bond between neighboring B atoms. For YB_{12}, this is the intercuboctahedral B-B bond. The

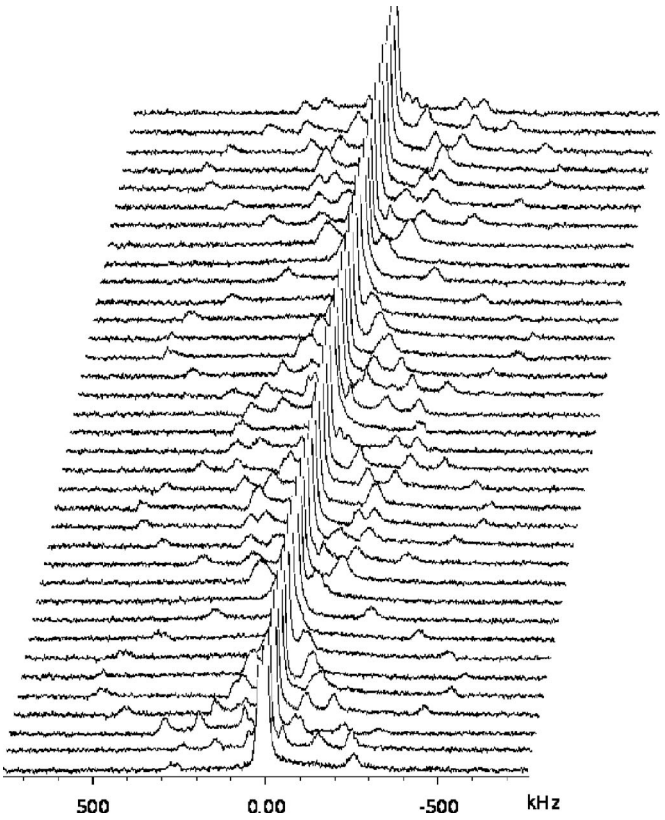

FIG. 1. ^{11}B NMR spectra obtained for different rotation angles for a single crystal of YB_{12}.

positions of the particular boron atoms in the cluster are shown in more detail in Fig. 4. The orientation of the EFG tensor for B(1) was calculated earlier[10] by first-principles methods. Now, taking into account symmetry arguments, Table I was created. From the known principal axes for one boron atom, the orientations of the axes for the other atoms are obtained by applying symmetry operations. Although six

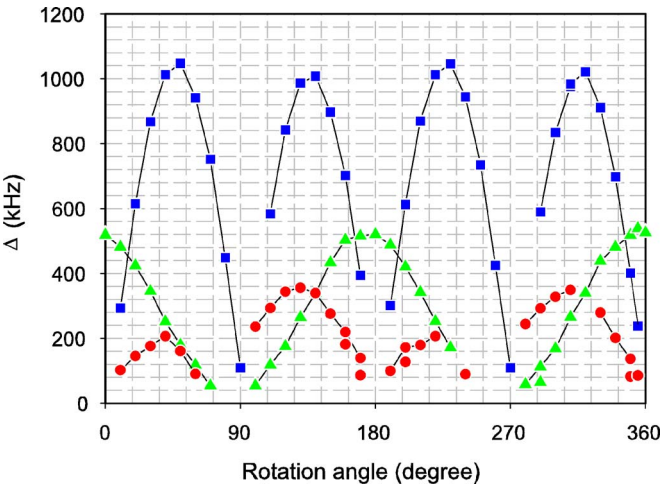

FIG. 2. (Color online) The separation between satellite lines in YB_{12} as a function of the rotation angle. The solid lines are only guides for the eyes. The filled circles, squares, and triangles correspond to the pairs of satellites arising from the B atoms denoted {1,2,3,4}, {5,6,7,8}, and {9,10,11,12}, respectively, in Fig. 4.

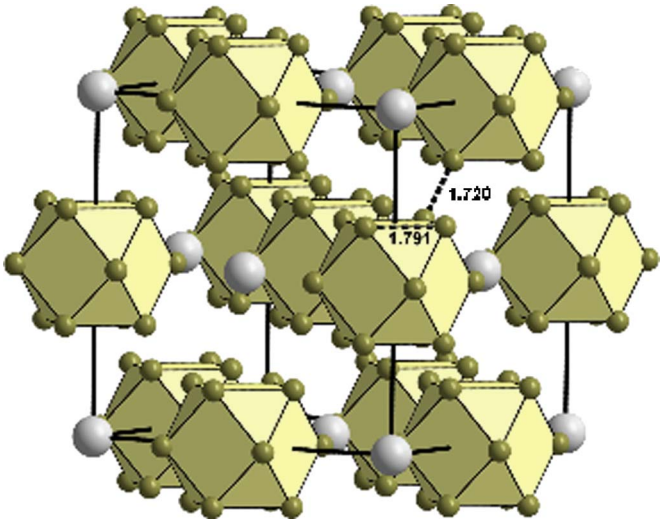

FIG. 3. (Color online) The crystal structure of YB_{12}. B-B distances (in Å) for the inter- and intra-B_{12}-cluster bonds in YB_{12}. These distances correspond to a lattice parameter of 7.500 Å for the cubic unit cell.

satellite pairs are anticipated from Table I, in the NMR experiment this number is reduced for particular values of the polar angles θ and ϕ.

The rotation pattern for each pair can be calculated using Eq. (1) when ν_Q, η, and the orientation of the principal axes are known. In what follows, we used ν_Q and η as free parameters and the polar angles θ and ϕ have been calculated using the procedure described below. These angles depend on the orientation of the principal axes through a unit vector $\boldsymbol{b}$, which defines the direction of the magnetic field with respect to the principal axes. Let $\boldsymbol{p}_1,\boldsymbol{p}_2,\boldsymbol{p}_3$ (Fig. 5) be the orthogonal unit vectors in the direction of the principal axes p_1,p_2,p_3. A rotation of the crystal is equivalent to a rotation of the principal axes for the electric-field gradient. When the crystal is rotated by an angle α, the vectors $\boldsymbol{p}_i$ are transformed into $\boldsymbol{p}_{i,\alpha}$ $(i=1,2,3)$, which are given by

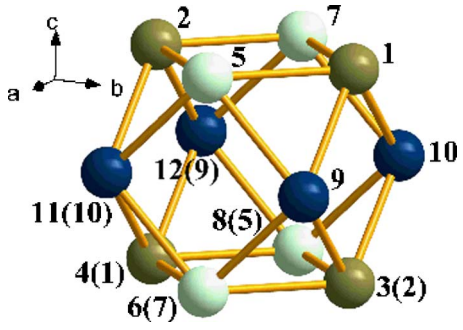

FIG. 4. (Color online) The B_{12} cluster in YB_{12}. The numbers are the site numbers (see Table I); those in round brackets refer to the corresponding sites to which they are related by the inversion of space through the center of the cuboctahedron. The B atoms represented by the same shade lead to satellite separation curves which are identical (inversion symmetry) or cannot be completely resolved due to limitations in the experimental resolution.

TABLE I. The principal axes for the EFG at the different B sites in YB_{12}.

Site No.	B coordinates	$\boldsymbol{p}_1$	$\boldsymbol{p}_2$	$\boldsymbol{p}_3$
1,4	$\frac{1}{2},x,x;\ \frac{1}{2},\bar{x},\bar{x}$	(1,0,0)	$\left(0,\frac{1}{\sqrt{2}},\frac{1}{\sqrt{2}}\right)$	$\left(0,-\frac{1}{\sqrt{2}},\frac{1}{\sqrt{2}}\right)$
2,3	$\frac{1}{2},\bar{x},x;\ \frac{1}{2},x,\bar{x}$	(1,0,0)	$\left(0,\frac{1}{\sqrt{2}},-\frac{1}{\sqrt{2}}\right)$	$\left(0,\frac{1}{\sqrt{2}},\frac{1}{\sqrt{2}}\right)$
5,8	$x,\frac{1}{2},x;\ \bar{x},\frac{1}{2},\bar{x}$	(0,1,0)	$\left(\frac{1}{\sqrt{2}},0,\frac{1}{\sqrt{2}}\right)$	$\left(-\frac{1}{\sqrt{2}},0,\frac{1}{\sqrt{2}}\right)$
6,7	$\bar{x},\frac{1}{2},x;\ x,\frac{1}{2},\bar{x}$	(0,1,0)	$\left(\frac{1}{\sqrt{2}},0,-\frac{1}{\sqrt{2}}\right)$	$\left(\frac{1}{\sqrt{2}},0,\frac{1}{\sqrt{2}}\right)$
9,12	$x,x,\frac{1}{2};\ \bar{x},\bar{x},\frac{1}{2}$	(0,0,1)	$\left(\frac{1}{\sqrt{2}},\frac{1}{\sqrt{2}},0\right)$	$\left(-\frac{1}{\sqrt{2}},\frac{1}{\sqrt{2}},0\right)$
10,11	$\bar{x},x,\frac{1}{2};\ x,\bar{x},\frac{1}{2}$	(0,0,1)	$\left(\frac{1}{\sqrt{2}},-\frac{1}{\sqrt{2}},0\right)$	$\left(\frac{1}{\sqrt{2}},\frac{1}{\sqrt{2}},0\right)$

$$\boldsymbol{p}_{i,\alpha}=\cos\alpha\boldsymbol{p}_i+\sin\alpha(\boldsymbol{r}\times\boldsymbol{p}_i)+(1-\cos\alpha)(\boldsymbol{r}\cdot\boldsymbol{p}_i)\boldsymbol{r}. \quad (2)$$

This formula[14] describes the rotation of a vector $\boldsymbol{p}_i$ about the axis of a unit vector $\boldsymbol{r}$ by an angle α. This transformation is called a conical transformation.[14] The angles θ and ϕ, which depend on the orientation of the principal axes relative to the vector $\boldsymbol{b}$, can be expressed in terms of the angle α:

$$\cos\theta=\boldsymbol{p}_{3,\alpha}\cdot\boldsymbol{b},\quad \tan\phi=(\boldsymbol{p}_{2,\alpha}\cdot\boldsymbol{b})/(\boldsymbol{p}_{1,\alpha}\cdot\boldsymbol{b}). \quad (3)$$

Now, the calculation of the quadrupole splittings can be made using the $\boldsymbol{p}_1,\boldsymbol{p}_2,\boldsymbol{p}_3$ vectors given in Table I and choosing appropriate values for ν_Q and η. The results of these calculations together with experimental data are shown in Figs. 6–8. The values $\nu_Q=540$ kHz and $\eta=0.94$ were used in our calculations. These values are very close to those (532 kHz and 0.93) previously obtained[10] from the measurements of the quadrupole splittings in a powder sample. The asymmetry parameter $\eta=0.93$ and the ν_Q values of 593 and 526 kHz were calculated from first principles using $Q(^{11}\mathrm{B})=0.04$ and 0.0355 b, respectively. Both values for $Q(^{11}\mathrm{B})$ can be found in the literature.[15,16]

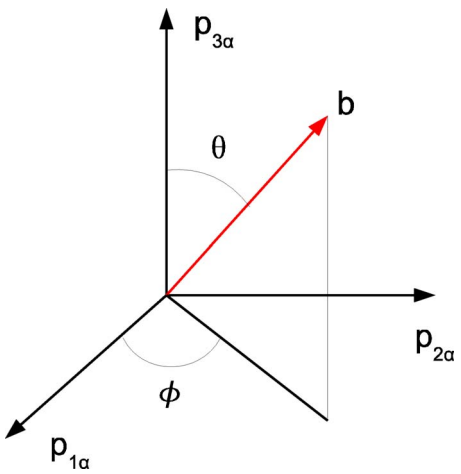

FIG. 5. (Color online) The angles θ and ϕ as defined by the orientation of the vector $\boldsymbol{b}$ with respect to the principal axes.

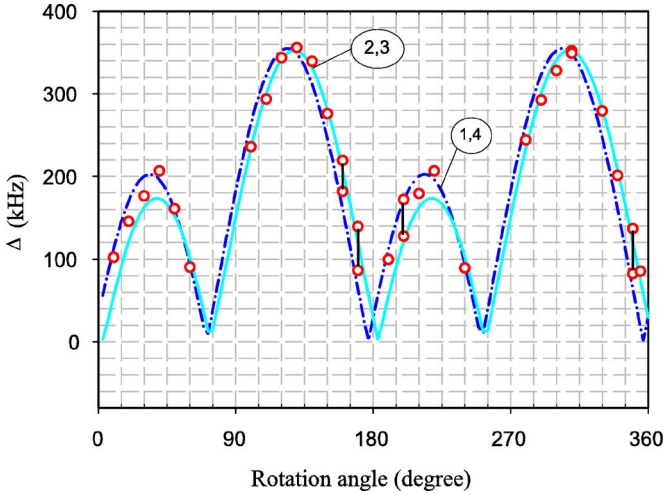

FIG. 6. (Color online) Satellite separations for the ^{11}B atoms in YB_{12} at sites 1,4 and 2,3 (see Fig. 4 and Table I). Circles and squares designate experimental results; the curves are obtained from calculations (using ν_Q=540 kHz and η=0.94). Vertical lines for the 160°, 170°, 200°, and 350° angles indicate experimentally observed differences between the B atoms at the 1,4 and 2,3 sites.

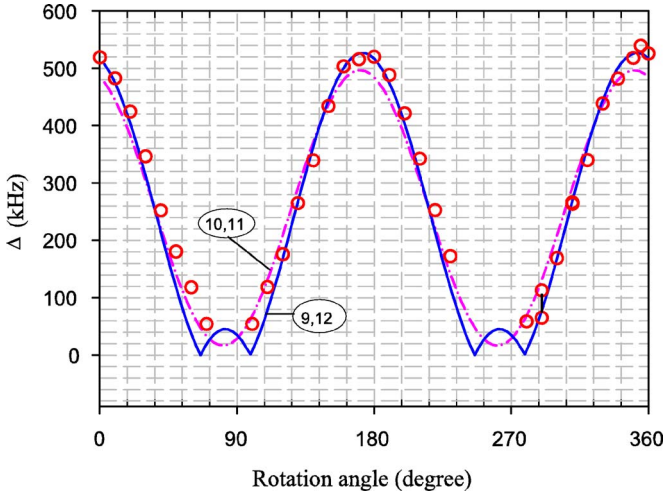

FIG. 8. (Color online) Satellite separations for the ^{11}B atoms in YB_{12} at sites 9,12 and 10,11 (see Fig. 4 and Table I). Circles designate experimental results; the curves are obtained from calculations (using ν_Q=540 kHz and η=0.94). The vertical line at 290° indicates the experimentally observed difference between the B atoms at the 10,11 and 9,12 sites.

It is worth noting the very good agreement between experimental and calculated values. The results indicate that the rotation patterns for certain crystallographic positions are very close. This can be seen particularly well for the B sites 5–8 (Figs. 4 and 7). Consequently, we observe only three pairs of satellites instead of six as one would expect from inspection of Table I. For four angles (α=160°, 170°, 200°, and 350°) as shown in Fig. 6 and one angle (α=290°) in Fig. 8, however, the resolution is good enough to identify further pairs of satellites. An even better resolution would require a better quality of the crystal. Imperfections of the crystal created by disorder, dislocations, strains, vacancies, interstitials, and foreign atoms at the positions of some of the nuclei create additional electric-field gradients, which vary not only with orientation but also in magnitude from site to site and have a considerable influence on the linewidths and intensities of the satellites even in first-order perturbation theory. The existence of such effects is noticeable in our crystal if one compares the intensity of the central transition ($-1/2 \leftrightarrow 1/2$) with the intensities of the satellites. The relative intensities of the satellites are remarkably lower than those predicted by theory.[17]

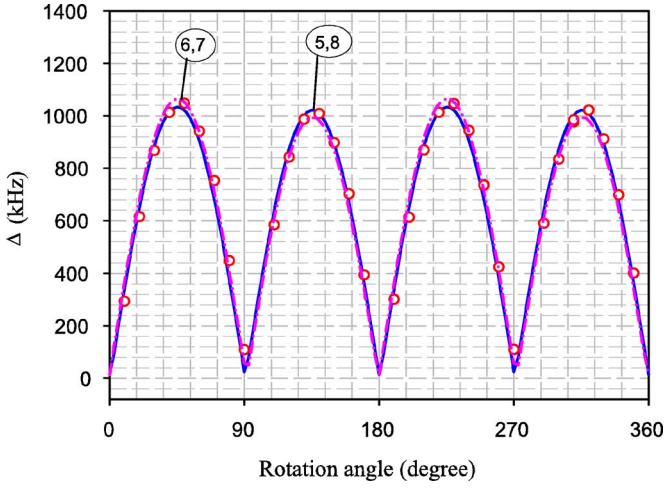

FIG. 7. (Color online) Satellite separations for the ^{11}B atoms in YB_{12} at sites 5,8 and 6,7 (see Fig. 4 and Table I). Circles designate experimental results; the curves are obtained from calculations (using ν_Q=540 kHz and η=0.94).

IV. CONCLUSIONS

The ^{11}B NMR experiments on a single crystal of yttrium dodecaboride have demonstrated the possibility to observe and distinguish the satellites coming from the different boron sites, which are crystallographically equivalent but magnetically nonequivalent. The distinction can be made because of the site dependence of the EFG-tensor orientation in space with respect to the magnetic field. The resolution among six anticipated pairs depends on the EFG-tensor orientation. For the crystal orientation used in the reported measurements, three pairs of satellites can easily be distinguished. From the angular dependence of the quadrupole splittings, which are in agreement with experimental observations, the boron groups to which they correspond can be identified. The ν_Q and η values reported here agree very well with those previously determined from ^{11}B NMR experiments on powder samples of YB_{12}, and the EFG-tensor orientations calculated by first-principles methods have been confirmed experimentally by the ^{11}B NMR measurements reported here.

ACKNOWLEDGMENTS

This work has been partly supported by INTAS Project No. 03-51-3036 and by the Austrian Science Fund (Project No. 15801-N02).

[1] P. Herzig, Theor. Chim. Acta **67**, 323 (1985).
[2] P. Blaha, K. Schwarz, and P. Herzig, Phys. Rev. Lett. **54**, 1192 (1985).
[3] H. Haas, Hyperfine Interact. **136/137**, 731 (2001).
[4] K. Schwarz, H. Ripplinger, and P. Blaha, Z. Naturforsch., A: Phys. Sci. **51A**, 527 (1996).
[5] T. J. Bastow, Solid State Commun. **124**, 269 (2002).
[6] S. H. Baek, B. J. Suh, E. Pavarini, F. Borsa, R. G. Barnes, S. L. Bud'ko, and P. C. Canfield, Phys. Rev. B **66**, 104510 (2002).
[7] N. I. Medvedeva, A. L. Ivanovskii, J. E. Medvedeva, A. J. Freeman, and D. L. Novikov, Phys. Rev. B **65**, 052501 (2002).
[8] P. Ravindran, P. Vajeeston, R. Vidya, A. Kjekshus, and H. Fjellvåg, Phys. Rev. B **64**, 224509 (2001).
[9] B. Jäger, S. Paluch, W. Wolf, P. Herzig, O. J. Żogał, N. Shitsevalova, and Y. Paderno, J. Alloys Compd. **383**, 232 (2004).
[10] B. Jäger, S. Paluch, O. J. Żogał, W. Wolf, P. Herzig, V. B. Filippov, N. Shitsevalova, and Y. Paderno, J. Phys.: Condens. Matter **18**, 2525 (2006).
[11] T. I. Serebryakova, V. A. Neronov, and P. D. Peshev, *Vysokotemperaturnye Boridy* (Metallurgiya, Moscow, 1991).
[12] N. Shishiuchi, Y. Kato, O. M. Vyaselev, M. Takigawa, S. Hiura, F. Iga, and T. Takabatake, J. Phys. Chem. Solids **63**, 1231 (2002).
[13] V. I. Matkovich, J. Economy, R. F. Giese, Jr., and R. Barrett, Acta Crystallogr. **19**, 1056 (1965).
[14] S. L. Altmann, *Rotations, Quaternions, and Double Groups* (Clarendon, Oxford, 1986), p. 163.
[15] B. C. Gerstein and C. R. Dybowski, *Transient Techniques in NMR of Solids* (Academic, New York, 1985).
[16] P. Pyykkö, Z. Naturforsch., A: Phys. Sci. **47A**, 189 (1992).
[17] A. Abragam, *The Principles of Nuclear Magnetism* (Oxford University Press, New York, 1961), p. 234.